Implementation of a Toffoli Gate with Superconducting Circuits

A. Fedorov,[1] L. Steffen,[1] M. Baur,[1] and A. Wallraff[1]

[1] *Department of Physics, ETH Zurich, CH-8093 Zurich, Switzerland*

(Dated: August 22, 2011)

The quantum Toffoli gate allows universal reversible classical computation. It is also an important primitive in many quantum circuits and quantum error correction schemes. Here we demonstrate the realization of a Toffoli gate with three superconducting transmon qubits coupled to a microwave resonator. By exploiting the third energy level of the transmon qubit, the number of elementary gates needed for the implementation of the Toffoli gate, as well as the total gate time can be reduced significantly in comparison to theoretical proposals using two-level systems only. We characterize the performance of the gate by full process tomography and Monte Carlo process certification. The gate fidelity is found to be $64.5 \pm 0.5\%$.

The Toffoli gate is a three-qubit operation that inverts the state of a target qubit conditioned on the state of two control qubits. It was originally proposed as a universal gate in the context of reversible computation [1]. Together with a Hadamard gate it forms a universal set of gates in quantum computation [2]. It is also one of the essential building blocks in quantum error correction schemes [3–7]. The quantum Toffoli gate has so far been implemented in nuclear magnetic resonance [3], linear optics [8] and ion trap systems [9]. Also, experiments with superconducting qubits have shown remarkable progress in recent years. Two-qubit algorithms [10, 11], generation of three-qubit entangled states [12, 13] and a teleportation protocol up to a measurement step [14] have been demonstrated. Implementation of the Toffoli gate with only single and two-qubit gates requires 6 CNOT gates and 10 single-qubit operations [15] and remains difficult to realize with superconducting qubits due to limited coherence. Making use of the third energy level of the transmon qubit we significantly reduce the number of elementary operations as well as the total gate time required to realize the Toffoli gate. The results reinforce the potential of macroscopic superconducting qubits for implementation of complex quantum operations and point at the possibility to implement quantum error correction schemes [16].

We have implemented a Toffoli gate with three transmon qubits (A,B,C) dispersively coupled to a microwave transmission line resonator as shown in Fig. 1(a,b). The resonator is used for joint three-qubit readout by measuring its transmission [17]. At the same time it serves as a coupling bus for the qubits [18]. The qubits have a ladder-type energy level structure with sufficient anharmonicity to allow individual microwave addressing of different transitions [Fig. 1(c)]. We utilize the first two levels as the computational qubit states $|0\rangle$ and $|1\rangle$, while the second excited state $|2\rangle$ is used to perform two-qubit and two-qutrit operations. From spectroscopy we deduce a bare resonator frequency $\nu_r = 8.625\,\mathrm{GHz}$ with a quality factor of 3300, maximum qubit transition frequencies $\nu^{\max}_{A,B,C} = \{6.714, 6.050, 4.999\}\,\mathrm{GHz}$, charging energies $E_c/h = \{0.264, 0.296, 0.307\}\,\mathrm{GHz}$ and coupling strengths $g/2\pi = \{0.36, 0.30, 0.34\}\,\mathrm{GHz}$ to the resonator. At $\nu^{\max}_{A,B,C}$ we find qubit energy relaxation times of $T_1 = \{0.55, 0.70, 1.10\}\,\mu\mathrm{s}$ and phase coherence times of $T_2^* = \{0.45, 0.6, 0.65\}\,\mu\mathrm{s}$.

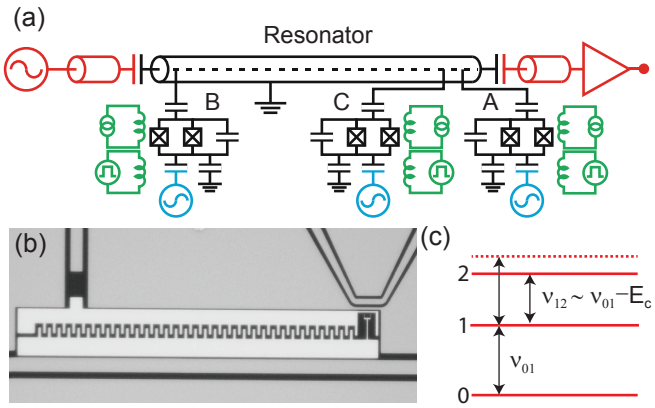

FIG. 1. a) Lumped element circuit diagram of sample and measurement setup. Qubits coupled to a transmission line resonator are shown in black. The red color indicates the circuitry used for transmission measurements. The blue and green lines depict local charge and flux controls. b) Optical microscope image of qubit B. The open transmission line is used to perform single qubit rotations with microwaves. The magnetic flux-bias line next to the SQUID loop of the qubit allows for frequency tuning on the nanosecond time scale. c) Energy level diagram for the transmon qubit.

In the conventional realization of the Toffoli gate, a NOT operation is applied to the target qubit (C) if the control qubits (A, B) are in the state $|11\rangle$. In our setup it is more natural to construct a variation of the Toffoli gate shown in Fig. 2(a) where the state of the target qubit is inverted if the control qubits are in $|01\rangle$. This gate can easily be transformed to the conventional Toffoli gate by a redefinition of the computational basis states of qubit A or by adding two π-pulses on qubit A.

The Toffoli gate can be constructed from a controlled-controlled-phase gate (CCPHASE) sandwiched between two single-qubit gates acting on the target qubit as shown in Fig. 2b. A CCPHASE gate leads to a π phase shift for

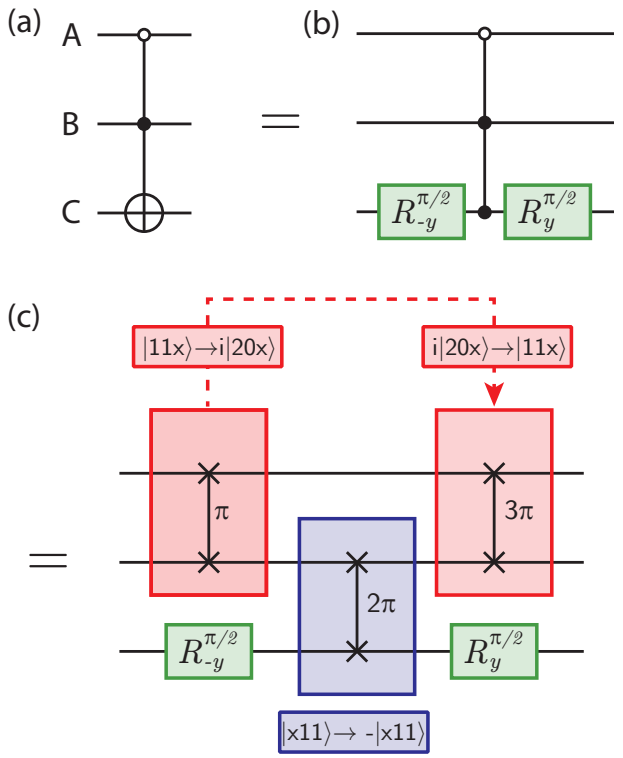

FIG. 2. Circuit diagram of the Toffoli gate. (a) A NOT-operation ($\oplus$) is applied to qubit C if the control qubits (A,B) are in the ground ($\circ$) and excited state ($\bullet$) respectively. (b) The Toffoli gate can be decomposed into a CCPHASE-gate and $\pm\pi/2$ rotations about the y-axis (green) of qubit C. (c) The CCPHASE-gate is implemented as three two-qubit/qutrit gates, where the $|11\rangle$ state is tuned into resonance with $|20\rangle$ for a $\{\pi, 2\pi, 3\pi\}$ SWAP respectively.

the $|1\rangle$ state of the target qubit if the control qubits are in the state $|01\rangle$. In other words, this corresponds to a sign change of only one out of the 9 computational three-qubit basis states: $|011\rangle \leftrightarrow -|011\rangle$.

The most efficient decomposition of the Toffoli gate using only two-level systems requires 6 CNOT gates and multiple single-qubit operations. The basic idea of 'hiding' states into non-computational states to simplify the implementation of a Toffoli gate was theoretically proposed in Ref. [15] and experimentally implemented for linear optics and ion trap systems [8, 9]. The implementation of the scheme of Ref. [15] in our setup would require 3 CPHASE gates, 6 single-qubit and 2 single-qutrit operations. Instead, we construct the controlled phase gate from a single two-qubit CPHASE gate and two two-qutrit gates denoted as a π-SWAP and a 3π-SWAP shown in Fig. 2c. The application of a single CPHASE gate on qubits B and C (shown in blue frame) inverts the sign of both the $|111\rangle$ and $|011\rangle$ states. To create the CCPHASE operation the computational basis state $|111\rangle$ is transferred to the non-computational state $i|201\rangle$ by the first π-SWAP (shown in left red frame), effectively 'hiding' it from the CPHASE operation acting on qubits B and C. After the CPHASE operation, the $|111\rangle$ state is recovered from the non-computational level $i|201\rangle$ by an additional 3π-SWAP. The utilization of two-qutrit instead of single-qutrit operations allows for a more efficient construction of the Toffoli gate with only half of the duration in comparison to the schemes described before.

All three-qubit basis states show three distinct evolution paths during our CCPHASE gate (see also Tab. I). Only the input state $|011\rangle$ is affected by CPHASE gate acting on qubits B and C which transfers $|011\rangle$ to the desired state $-|011\rangle$. The states $|11x\rangle$ ($x \in \{0, 1\}$) are transferred by the π-SWAP gate to the states $i|20x\rangle$. The following CCPHASE gate then has no influence on the resulting state. The last gate, a 3π-SWAP, transfers $i|20x\rangle$ back to $|11x\rangle$. The two swap gates (π and 3π) realize a full 4π rotation such that the state $|11x\rangle$ does not acquire any extra phase compared to the other states. The states of the last group ($|010\rangle, |x0y\rangle$ with $y \in \{0, 1\}$) do not change during the CPHASE gate sequence.

The actual experimental implementation of the Toffoli gate consists of a sequence of microwave and flux pulses applied to the qubit local control lines [Fig. 3]. The arbitrary rotations about the x and y axis [19] are realized with resonant microwave pulses applied to the open transmission line at each qubit, see Fig. 1(a,b). We use 8 ns long Gaussian shaped DRAG-pulses [19, 20] to prevent population of the third level during the single-qubit operations. Few nanosecond long current pulses passing through the transmission line next to the SQUID loop of the respective qubits control the qubit transition frequency realizing z-axis rotations. All two-qubit/qutrit gates are implemented by tuning a qutrit non-adiabatically to the avoided crossing between the $|11x\rangle \leftrightarrow |20x\rangle$ or $|x11\rangle \leftrightarrow |x20\rangle$ states, respectively [12, 21]. During this time the system oscillates between the states with a frequency $2J_{11,20}^{AB/BC}$. Depending on the interaction time $t = \{\pi, 2\pi, 3\pi\}/2J_{11,20}^{AB/BC} = \{7, 23, 20\}$ ns, the corresponding final states are $i|20\rangle, -|11\rangle$, and $-i|20\rangle$, thus realizing a π-SWAP, CPHASE, and 3π-SWAP gate, respectively.

During the flux pulses the transition frequencies of the

Initial state	after π-SWAP	after CPHASE	after 3π-SWAP
$\|011\rangle$	$\|011\rangle$	$-\|011\rangle$	$-\|011\rangle$
$\|110\rangle$	$i\|200\rangle$	$i\|200\rangle$	$\|110\rangle$
$\|111\rangle$	$i\|201\rangle$	$i\|201\rangle$	$\|111\rangle$
$\|x0y\rangle$	$\|x0y\rangle$	$\|x0y\rangle$	$\|x0y\rangle$
$\|010\rangle$	$\|010\rangle$	$\|010\rangle$	$\|010\rangle$

TABLE I. List of states after each step of the CCPHASE gate. The state $|011\rangle$ acquires a π phase shift during the CPHASE pulse, the states $|11x\rangle$ are transferred to $i|20x\rangle$, 'hiding' it from the CPHASE gate, the initial states $|x0y\rangle$ and $|010\rangle$ do not change during the sequence.

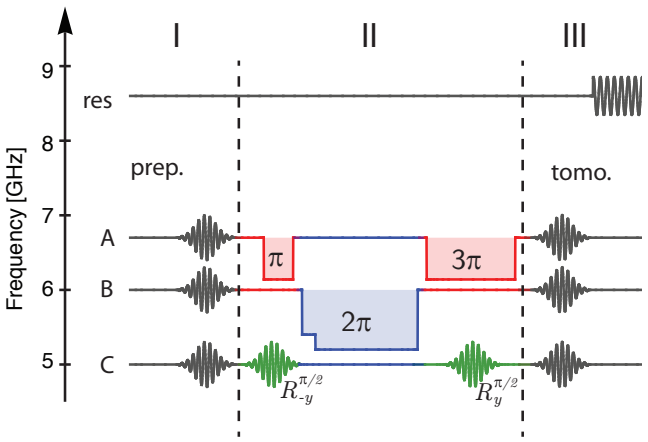

FIG. 3. Illustration of the pulse sequence used for the implementation of the Toffoli gate. During the preparation (I) resonant microwave pulses are applied to the qubits on the corresponding gate lines. The Toffoli gate (II) is implemented with three flux pulses and resonant microwave pulses (color code as in Fig. 2). The measurement (III) consists of microwave pulses that turn the qubit states to the desired measurement axis and a subsequent microwave pulse applied to the resonator is used for performing a joint dispersive read out.

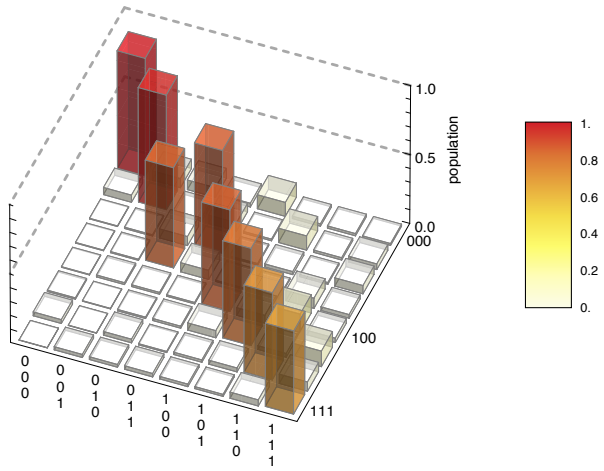

FIG. 4. Truth table of the Toffoli gate: The state of a qubit C is inverted if qubits A and B are in the state $|01\rangle$. Fidelity of the truth table is $F = (1/8)\mathrm{Tr}\left[U_{\mathrm{exp}}^{T} U_{\mathrm{ideal}}\right] = 76.0\%$

qubits are shifted which results in dynamic phases acquired by the qubits. These phases are canceled by adjusting the rotation axes of the subsequent single-qubit pulses. A short flux pulse applied on qubit B before the CPHASE gate is used to compensate the remaining dynamic phase which is acquired by the state $|11x\rangle$ when it is 'hidden' in the state $i|20x\rangle$.

We have characterized the performance of this realization of a Toffoli gate by measuring the truth table, by full process tomography [22] and by Monte Carlo process certification [23]. The truth table depicted in Fig. 4 shows the population of all computational basis states after applying the Toffoli gate onto each of the computational basis states. It clearly reveals the characteristic properties of the Toffoli gate, namely that a NOT operation is applied on the target qubit (C) if the control qubits (A,B) are in the state $|01\rangle$. The fidelity of the output states show a significant dependence on qubit lifetime. In particular, input states with qubit A (with the shortest lifetime) in the excited state exhibit generally the worst fidelity, indicating that the protocol is mainly limited by the qubit lifetime. The fidelity of the measured truth table is $F = (1/8)\mathrm{Tr}\left[U_{\mathrm{exp}}^{T} U_{\mathrm{ideal}}\right] = 76.0\%$

We performed full process tomography and reconstruct the process matrix χ_{exp} to completely characterize the Toffoli gate including its non-classical features. For this purpose we prepared a complete set of 64 distinct input states by applying all combinations of single-qubit operations chosen from the set $\{\mathrm{id}, \pi/2_x, \pi/2_y, \pi_x\}$ for each qubit and performed state tomography on the respective output states. The reconstructed process matrix χ_{exp} has a fidelity of $F = \mathrm{Tr}[\chi_{\mathrm{exp}}^{T}\chi_{\mathrm{ideal}}] = 70\%$ but is subject to noise and therefore shows unphysical properties such as small negative eigenvalues. We apply the maximum likelihood procedure [24] to correct for unphysical properties of χ_{exp}. The obtained physical process matrix $\chi_{\mathrm{exp}}^{\mathrm{ML}}$ gives a fidelity of $F = \mathrm{Tr}[\chi_{\mathrm{exp}}^{T}\chi_{\mathrm{ideal}}] = 69\%$ and is shown in Fig. 5 in comparison to the ideal process matrix χ_{ideal}.

For an accurate alternative estimate of the process fidelity without resorting to a maximum likelihood procedure we implemented Monte Carlo process certification [23]. First we define a Pauli observable as $\hat{P}_n = \prod_{j=1,\ldots,6}^{\otimes} \hat{p}_j$, a product of 6 single-qubit operators chosen from the set of the identity and the Pauli operators ($\hat{p}_j \in \{\mathbb{1}, \sigma_x, \sigma_y, \sigma_z\}$). Then we determine the 232 observables with non-vanishing expectation values $P_n = \mathrm{Tr}[\hat{\rho}_T \hat{P}_n] \neq 0$, where $\hat{\rho}_T$ is Choi matrix of the Toffoli process. For each $\hat{P}_n$ we prepare all ($2^3 = 8$) eigenstates of the product of the first 3 operators comprised in $\hat{P}_n$, apply the Toffoli operation on this state and measure the expectation value of the product of the last 3 operators in $\hat{P}_n$. Averaging over the results obtained with all eigenstates provides an estimate of P_n. Extracting all 232 expectation values P_n allows us to estimate the fidelity of the Toffoli gate as $64.5 \pm 0.5\%$ (the error represents a 90% confidence interval), which is in good agreement with the fidelity evaluated by a process tomography.

In summary we have experimentally implemented a Toffoli gate with three superconducting transmon qubits, constructed from two microwave single-qubit rotations, a single two-qubit and two two-qutrit operations. By encoding computational states into higher levels of the transmon qubit we reduce the total gate time to 90 ns,

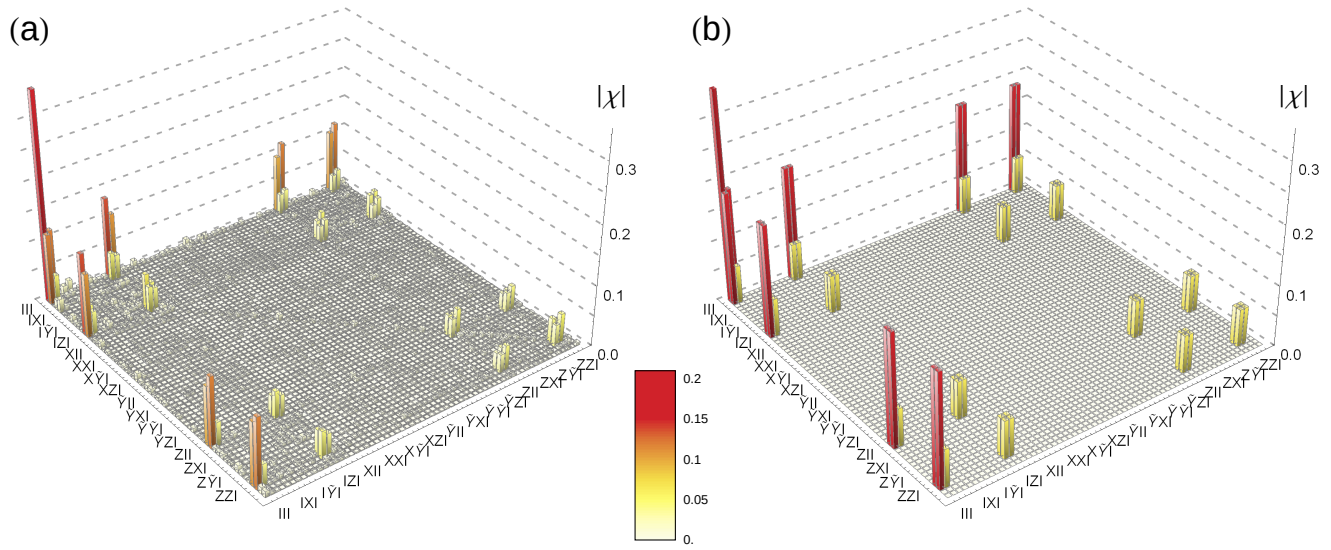

FIG. 5. Bar chart of the absolute value of the measured process matrix $\chi_{\rm exp}^{\rm ML}$ (a) and ideal process matrix $\chi_{\rm ideal}$-matrix (b). The elements are displayed in the operator basis $\{III, IIX, II\tilde{Y}, \ldots ZZZ\}$, where $\{I, X, \tilde{Y}, Z\}$ are the identity and Pauli operators $\{\mathbb{1}, \sigma_x, -i\sigma_y, \sigma_z\}$. The fidelity of the process matrix is $F = {\rm Tr}[\chi_{\rm exp}^T \chi_{\rm ideal}] = 69\%$. The process fidelity estimated with the Monte Carlo certification method is $64.5 \pm 0.5\%$.

twice shorter, than with previously proposed scheme based on single-qutrit operations.

We thank Marcus da Silva for providing support on using the Monte Carlo process certification, Stefan Filipp, Alexandre Blais for useful discussions and Kiryl Pakrouski for his contributions in early stages of the experimental work. This work was supported by the Swiss National Science Foundation (SNF), the EU IP SOLID and ETH Zurich.

[1] T. Toffoli, *Automata, Languages and Programming*, edited by J. de Bakker and J. van Leeuwen, Lecture Notes in Computer Science, Vol. 85 (Springer Berlin / Heidelberg, 1980) pp. 632–644.
[2] Y. Shi, arXiv:0205115 (2002).
[3] D. G. Cory, M. D. Price, W. Maas, E. Knill, *et al.*, Phys. Rev. Lett. **81**, 2152 (1998).
[4] E. Knill, R. Laflamme, R. Martinez, and C. Negrevergne, Phys. Rev. Lett. **86**, 5811 (2001).
[5] J. Chiaverini, D. Leibfried, T. Schaetz, M. Barrett, *et al.*, Nature **432**, 602 (2004).
[6] T. B. Pittman, B. C. Jacobs, and J. D. Franson, Phys. Rev. A **71**, 052332 (2005).
[7] T. Aoki, G. Takahashi, T. Kajiya, J.-i. Yoshikawa, *et al.*, Nat Phys **5**, 541 (2009).
[8] B. P. Lanyon, M. Barbieri, M. P. Almeida, T. Jennewein, *et al.*, Nat. Phys. **5**, 134 (2009).
[9] T. Monz, K. Kim, W. Hänsel, M. Riebe, *et al.*, Phys. Rev. Lett. **102**, 040501 (2009).
[10] L. DiCarlo, J. M. Chow, J. M. Gambetta, L. S. Bishop, *et al.*, Nature **460**, 240 (2009).
[11] T. Yamamoto, M. Neeley, E. Lucero, R. C. Bialczak, *et al.*, Phys. Rev. B **82**, 184515 (2010).
[12] L. DiCarlo, M. D. Reed, L. Sun, B. R. Johnson, *et al.*, Nature **467**, 574 (2010).
[13] M. Neeley, R. C. Bialczak, M. Lenander, E. Lucero, *et al.*, Nature **467**, 570 (2010).
[14] M. Baur, A. Fedorov, L. Steffen, S. Filipp, *et al.*, arXiv:1107.4774 (2011).
[15] T. C. Ralph, K. J. Resch, and A. Gilchrist, Phys. Rev. A **75**, 022313 (2007).
[16] To our knowledge, experimental work on the implementation of quantum error correction is in progress at Yale University.
[17] S. Filipp, P. Maurer, P. J. Leek, M. Baur, *et al.*, Phys. Rev. Lett. **102**, 200402 (2009).
[18] J. Majer, J. M. Chow, J. M. Gambetta, J. Koch, *et al.*, Nature **449**, 443 (2007).
[19] J. M. Gambetta, F. Motzoi, S. T. Merkel, and F. K. Wilhelm, Phys. Rev. A **83**, 012308 (2011).
[20] F. Motzoi, J. M. Gambetta, P. Rebentrost, and F. K. Wilhelm, Phys. Rev. Lett. **103**, 110501 (2009).
[21] F. W. Strauch, P. R. Johnson, A. J. Dragt, C. J. Lobb, *et al.*, Phys. Rev. Lett. **91**, 167005 (2003).
[22] I. L. Chuang and M. A. Nielsen, J. Mod. Opt. **44**, 2455 (1997).
[23] M. P. da Silva, O. Landon-Cardinal, and D. Poulin, arXiv:1104.3835 (2011).
[24] M. Ježek, J. Fiurášek, and Z. c. v. Hradil, Phys. Rev. A **68**, 012305 (2003).